Metal-insulator transition in the spinel-type CuIr$_2$(S$_{1-x}$Se$_x$)$_4$ system

Shoichi Nagata,* Nobuhiro Matsumoto, and Yoshiaki Kato

Department of Materials Science and Engineering, Muroran Institute of Technology, 27-1 Mizumoto-cho, Muroran, Hokkaido 050-8585, Japan

Takao Furubayashi and Takehiko Matsumoto

National Research Institute for Metals, 1-2-1 Sengen, Tsukuba, 305-0047, Japan

Jean Pierre Sanchez and Paul Vulliet

Département de Recherche Fondamentale sur la Matière Condensée, SPSMS, CEA-Grenoble, 17 rue des Martyrs, 38054 Grenoble, Cedex 9, France

The thiospinel CuIr$_2$S$_4$ exhibits a temperature-induced metal-insulator (M-I) transition around 226 K, showing hysteresis on heating and cooling, that manifests itself as a gap in the electronic density of state with increasing electrical resistivity at low temperatures. Conversely, CuIr$_2$Se$_4$ remains metallic down to 0.5 K. We have successfully synthesized the spinel-type compound CuIr$_2$(S$_{1-x}$Se$_x$)$_4$ system. In order to see the effect of substitutions of Se at the S sites, we have carried out a systematic experimental study of structural, electrical, and magnetic properties of CuIr$_2$(S$_{1-x}$Se$_x$)$_4$. Mössbauer spectroscopy measurements of ^{193}Ir have been performed for CuIr$_2$S$_4$ and CuIr$_2$Se$_4$. The M-I transition of CuIr$_2$(S$_{1-x}$Se$_x$)$_4$ for $x \leq 0.15$ is accompanied by a structural transformation from tetragonal (low-temperature insulating phase) to cubic (high-temperature metallic phase) symmetry. With increasing Se concentration x, the sharp M-I transition shifts to lower temperature. The resistivity shows a monotonous increase with decreasing temperature for $0.17 \leq x \leq 0.78$ between 4.2 and 300 K, and the metallic state is recovered for $x \geq 0.80$. Magnetic susceptibility measurements show the jump at the M-I transition temperature with hysteresis on heating and cooling. The high-temperature metallic phase of CuIr$_2$S$_4$ shows Pauli paramagnetism, having a density of states at the Fermi level, $D(\epsilon_F) = 0.67$ states/eV atom. The insulating phase at low temperatures exhibits diamagnetism, and there is no localized magnetic moment. The Arrhenius regime is observed for the conductivity with a thermally activated process for $0 \leq x \leq 0.70$ in the insulating phase. There is a general trend toward increasing metallicity with increasing x, which is consistent with the magnetic susceptibility results. A possibility of a two-site model of different valence states for Ir ions in the insulating phase of CuIr$_2$S$_4$ will be discussed on the basis of the Mössbauer data. A phase diagram of temperature versus Se concentration x will be proposed for the CuIr$_2$(S$_{1-x}$Se$_x$)$_4$ system. The mechanism of the M-I transition remains enigmatic and is far from a complete picture. [S0163-1829(98)01535-5]

I. INTRODUCTION

Sulphospinels exhibit a wide variety of physical properties, which makes them interesting from a scientific point of view, while oxyspinels are in general semiconductors with antiferromagnetic interaction.[1] One ternary thiospinel CuIr$_2$S$_4$ has a cubic spinel structure at room temperature and has a lattice constant of $a = 9.847$ Å, as shown in Fig. 1. CuIr$_2$S$_4$ has the normal spinel structure where Cu ions occupy the A (tetrahedral) sites and Ir ions occupy the B (octahedral) sites. We have discovered a metal-insulator transition at $T_{\text{M-I}} = 226$ K in CuIr$_2$S$_4$.[2] An abrupt drop of the conductivity by nearly three orders of magnitude has been observed. This metal-insulator transition is associated with a structural phase transition from a cubic to a tetragonal symmetry with decreasing temperature.[3] The phase transition has been observed to be first order. Temperature-dependent photoemission spectroscopy has been studied.[4] The high-resolution spectra near the Fermi energy shows an opening of a band gap through the M-I transition. The photoemission and Cu nuclear magnetic resonance (NMR) (Ref. 5) measurements have verified that Cu ion has a monovalent state

of Cu$^+$ in the low-temperature insulating state. Therefore, we expect the mixed valence state of Ir^{3+} and Ir^{4+}. Theoretical band calculations also predict and support the monovalent state of Cu ions.[6,7]

The electrical resistivity in CuIr$_2$S$_4$ shows activated conduction with an activation energy of 4.7×10^{-2} eV between 140 and 200 K.[2,8] The magnetic susceptibility exhibits a sharp change near 228 K. The high-temperature metallic phase of CuIr$_2$S$_4$ reveals Pauli paramagnetism and the lower-temperature insulating phase has semiconductive behavior with a diamagnetic contribution due to the core electrons.[2,8] A sharp heat capacity anomaly is observed at 230.8 K. The enthalpy and entropy of the transition are found to be 3.50 kJ mol^{-1} and 15.6 JK^{-1} mol^{-1}, respectively.[2,8] The pressure dependence of the M-I transition has been observed, where the M-I transition temperature increases with increasing pressure.[9,3]

The origin and the driving force for the structural phase transition and the M-I transition of CuIr$_2$S$_4$ are not understood at the present time. A primitive explanation for the transition from the cubic to tetragonal symmetry is that the Jahn-Teller active Cu^{2+} ions at A sites give rise to the co-
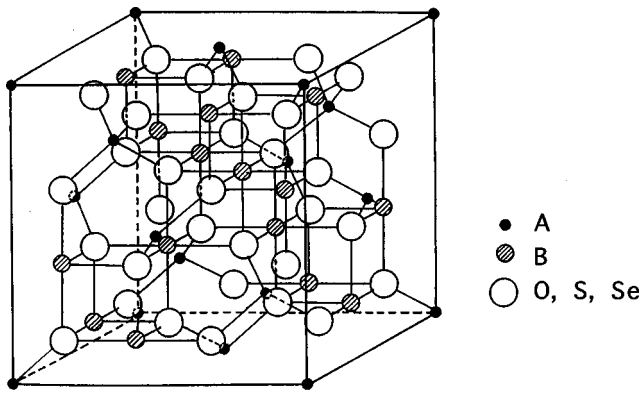
FIG. 1. The cubic unit cell of the spinel structure. Cu ions (A) lie on the tetrahedral site and Ir ions (B) on the octahedral sites. S or Se ions are indicated as open circles.

operative distortion. Nevertheless, this interpretation runs into a difficulty and has been denied because Cu ions have a monovalent state in the insulating phase.[4,5] Furthermore, the experimental result gives an axial ratio of $c/a = 1.03 > 1.0$ at 10 K for $CuIr_2S_4$, which indicates elongation along the c axis and the opposite distortion to that expected by the Jahn-Teller distortion for the $Cu^{2+}(d^9)$ in the tetrahedral site.

It is well known that magnetite Fe_3O_4 undergoes a phase transition (the Verwey transition) accompanied by a sudden change of conductivity at 119 K.[10–15] The Verwey transition in magnetite Fe_3O_4 has been studied extensively. The principal feature of the Verwey transition in magnetite has been simulated by adopting elements of order-disorder theory.[15] An ordering scheme of Fe^{2+} and Fe^{3+} ions on octahedral sites (B sites) is proposed. High conductivity of this oxide has been considered to be due to the hopping of electrons between these Fe^{2+} and Fe^{3+} ions on B sites. The electrical transition is clearly to be linked with a structural transformation. The comprehension of the charge ordering is, however, still far from a complete picture. Another candidate of the charge ordering system in a mixed valence state will be $CuIr_2S_4$, having the same spinel structure. One possibility, and the analogy for the mechanism in the M-I transition, will be pointed out.

On the other hand, another newly synthesized spinel $CuIr_2Se_4$ remains metallic down to 0.5 K.[16] The crystal structure of $CuIr_2Se_4$ is cubic symmetry at 10 K. The resistivity of $CuIr_2Se_4$ decreases gradually with decreasing temperature. The magnetic state is paramagnetic and the magnitude of the magnetic susceptibility, χ, is small and about -1.0×10^{-7} emu cm^{-3} with a weak temperature dependence ($d\chi/dT > 0$). The pressure dependence of the resistivity up to 5 GPa has been measured over a temperature range of 7–300 K.[17] The insulating phase is also induced and is stabilized with high pressure in $CuIr_2Se_4$. Thus, $CuIr_2Se_4$ at ambient pressure could be next door to the instability of the charge state and conductivity.

In order to see the effect of substitution of Se at the S site on the M-I transition, a systematic experimental study of structural, electrical, and magnetic properties of $CuIr_2(S_{1-x}Se_x)_4$ has been performed. The variation of Se concentration x leads to a systematic change of the magnetic and electrical features. In the range of $x < 0.17$, the abrupt

changes in the electrical and magnetic characteristics occur with the structural transformation, while for $x \geq 0.17$ it is emphasized that the physical properties are greatly altered without significant alteration of the cubic normal spinel structure solely by adjustment of the anion sublattice while the cation sublattice remains intact. A phase diagram between temperature and Se concentration x has been determined experimentally for the system of $CuIr_2(S_{1-x}Se_x)_4$.

Although some possible explanations of the metal-insulator transition in $CuIr_2(S_{1-x}Se_x)_4$ have been pointed out, the mechanism remains enigmatic and is still an open question. Further detailed study to clarify the novel phenomena is currently under way. It is our hope that the systematic measurements presented below for the system of $CuIr_2(S_{1-x}Se_x)_4$ will be helpful and lead to fruitful discussion. In addition, the Rh-based compounds, $CuRh_2S_4$ and $CuRh_2Se_4$, having the same normal spinel structure, become superconducting below transition temperatures of 4.70 and 3.48 K, respectively.[18–23] Some related investigations have been published.[24–28]

II. EXPERIMENTAL METHODS

A. Sample preparation and x-ray diffraction

The samples were prepared by a solid-state reaction:

$$Cu + 2Ir + 4(1-x)S + 4xSe \rightarrow CuIr_2(S_{1-x}Se_x)_4. \quad (1)$$
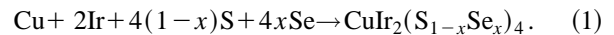
The starting materials, Cu (purity 99.99%), Ir (99.9%), S (99.999%), and Se (99.999%), were mixed in the calculated ratio. After mixing, they were sealed in an evacuated quartz tube with an extra 0.1 wt % of sulfur and selenium in the total weight of $CuIr_2(S_{1-x}Se_x)_4$ and heated to 1123 K for a period of 240 h. Subsequently, the resultant powder was reground and pressed into rectangular bars that were again heated to 1123 K for 48 h in the evacuated quartz tube. Single-phase products were obtained. The sintered specimens were very brittle and broken easily into some pieces.

The crystal structures and the lattice constants were determined by the powder x-ray diffraction method using Cu Kα radiation at room temperature and 10 K. The composition of the sample was analyzed with energy dispersive x-ray spectroscopy (EDX).

B. Measurements

Samples with dimensions of approximately $1.8 \times 1.8 \times 10$ mm^3 were used for the measurements of the electrical resistivity ρ. The resistivity was measured by a standard dc four-probe method in the temperature range 4.2–300 K. Silver paste was used to form the electrodes. The dc magnetic susceptibility was measured with a Quantum Design superconducting quantum interference device (rf-SQUID) magnetometer in a range of $5 \leq T \leq 300$ K at intervals of 5 K in an applied magnetic field of 10 kOe.

[193]Ir Mössbauer spectroscopy measurements ($3/2 \rightarrow 1/2$, 73 keV transition) were carried out using a [193]Os source produced by neutron irradiation of enriched [192]Os metal.[29,30] The source was always kept at 4.2 K while the absorber (~ 100 mg Ir/cm^2) was maintained at temperatures between 4.2 and 150 K. The velocity calibration of the spectrometer was performed using a [57]Co/Rh source and a me-
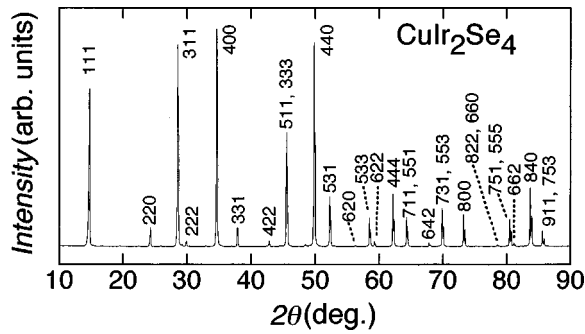
FIG. 2. X-ray diffraction pattern of a seleno spinel $CuIr_2Se_4$ that has the cubic structure with the lattice constant $a = 10.324$ Å and u parameter $u = 0.385$ at room temperature.

tallic iron absorber. The γ rays were counted with a high-resolution Ge detector. The spectra were least-squares analyzed taking into account the small quadrupolar interaction present in the source.

III. RESULTS AND DISCUSSION

A. X-ray analysis

The detailed experimental results of our x-ray analysis of $CuIr_2S_4$ have been reported by Furubayashi *et al.*[3] However, this spinel $CuIr_2Se_4$ does not show the structural transformation. So far there has been no information, to our knowledge, about x-ray data for $CuIr_2Se_4$ because of this compound. The powder x-ray diffraction pattern of $CuIr_2Se_4$ is shown in Fig. 2. All the powder diffraction peaks have been successfully indexed to the cubic unit cell with the spinel structure, which confirms the spinel structure and a single-phase sample. The lattice constant and u parameter are $a = 9.847$ Å and $u = 0.385$ for $CuIr_2S_4$ and $a = 10.324$ Å and $u = 0.385$ for $CuIr_2Se_4$ at room temperature. This lattice constant of $CuIr_2(S_{1-x}Se_x)_4$ varies linearly with the Se concentration x as shown in Fig. 3.

Over the concentration range of $x = 0$ to 0.15, the temperature-induced M-I transition is accompanied by a structural transformation from tetragonal symmetry in the insulating phase to cubic symmetry in the high-temperature metallic phase. The sharp change in the conductivity σ disappears about $x = 0.16$. Here we present only representative
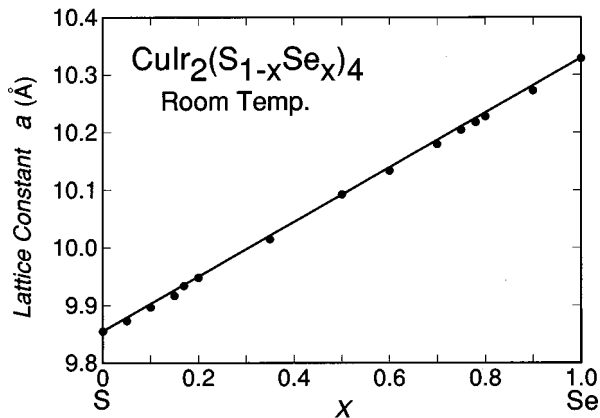

FIG. 3. The lattice constant a as a function of Se concentration x at room temperature.
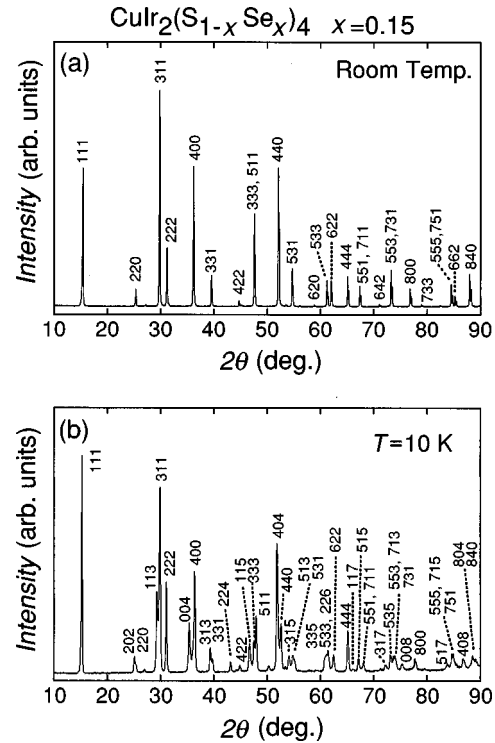

FIG. 4. X-ray diffraction pattern of $CuIr_2(S_{1-x}Se_x)_4$: $x = 0.15$, at room temperature (a) and 10 K (b). The diffraction patterns are completely different from each other, a cubic symmetry at (a) room temperature and (b) a tetragonal one at 10 K.

data of the x-ray measurements. Figures 4 and 5 show the powder x-ray diffraction patterns of $CuIr_2(S_{1-x}Se_x)_4$ at room temperature and 10 K, for $x = 0.15$ and 0.20, respectively. For $x = 0.15$, the sample undergoes the crystal transformation from tetragonal to cubic symmetry with changing temperature at approximately 174 K, having a temperature hysteresis. However, for $x = 0.20$, the sample remains cubic even at 10 K. Upon cooling and warming, the structural transformation occurs, at different temperatures as shown in Figs. 6 and 7 for $x = 0.05$ and 0.15, respectively. Both the cubic and tetragonal phases appear in a narrow temperature region. The coexistence of these phases and the hysteresis indicate a first-order phase transition. Furthermore, a supercooling effect has been observed clearly in the specific-heat measurement for $CuIr_2S_4$.[8]

B. Electrical resistivity

A systematic variation in the resistivity with x is shown in Fig. 8 for $CuIr_2(S_{1-x}Se_x)_4$. The expanded plots for the lower range of x are given in Figs. 9 and 10. The resistivity of $CuIr_2S_4$ increases abruptly from approximately 4.5 $\times 10^{-3}$ to 1.0 Ω cm at $T = 222$ K with decreasing temperature, while it decreases at $T = 230$ K with increasing temperature. The transition is slightly sharper upon cooling than warming. Whereas, $CuIr_2Se_4$ remains metallic down to 0.5 K without any anomaly. With increasing Se concentration x, the temperature-induced M-I transition temperature decreases steadily. The concentration-induced-like M-I transition is also found at approximately $x = 0.78$. The metallic state is recovered for $x \geqslant 0.80$. It should be noted that the
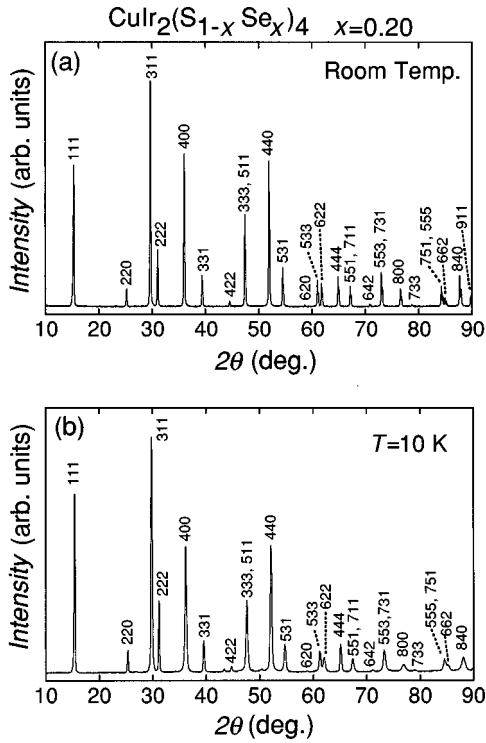
FIG. 5. X-ray diffraction pattern of $CuIr_2(S_{1-x}Se_x)_4$: $x = 0.20$, at (a) room temperature and (b) 10 K. The diffraction patterns are essentially the same.

temperature dependence of ρ above the M-I transition temperature changes from being positive in metallic behavior for $x \leq 0.08$ to being negative for $x \geq 0.08$.

Figure 11 shows the conductivity as a function of $1/T$ for $x \leq 0.70$. It is found that the conductivity data of insulating phase for $0 \leq x \leq 0.70$ could be analyzed in terms of the thermal excitation with the Arrhenius plot, which exhibits semiconducting behavior with a thermally activated conductivity, obeying the equation,

$$\sigma = A \exp(-q/k_B T). \qquad (2)$$

The slope of the $\ln \sigma$ versus $1/T$ plot gives an activation energy q. For $CuIr_2S_4$, the value of q is reported in earlier work.[2] Table I gives a summary numerical values of the activation energy q and the preexponential factor A for the various x of $CuIr_2(S_{1-x}Se_x)_4$.

On the other hand, at sufficiently low temperatures, below 50 K, an attempt has also been made to fit the σ versus T dependence in the insulating phase to Mott's formula derived for variable-range hopping (VRH),[31,32]

$$\sigma = \sigma_0 \exp(-B/T^{1/4}), \qquad (3)$$

where B is a constant. The experimental results are shown in Fig. 12 and they cannot be reproduced well by a single VRH formula over the entire region of the insulating phase. It is pointed out that the general tendency of our results in Fig. 12 is somewhat similar to that of Si:As samples for various concentrations.[33]

C. Magnetic susceptibility

Figure 13 shows the magnetic susceptibilities for $0.0 \leq x \leq 0.15$. These jumps also exhibit the temperature hysteresis
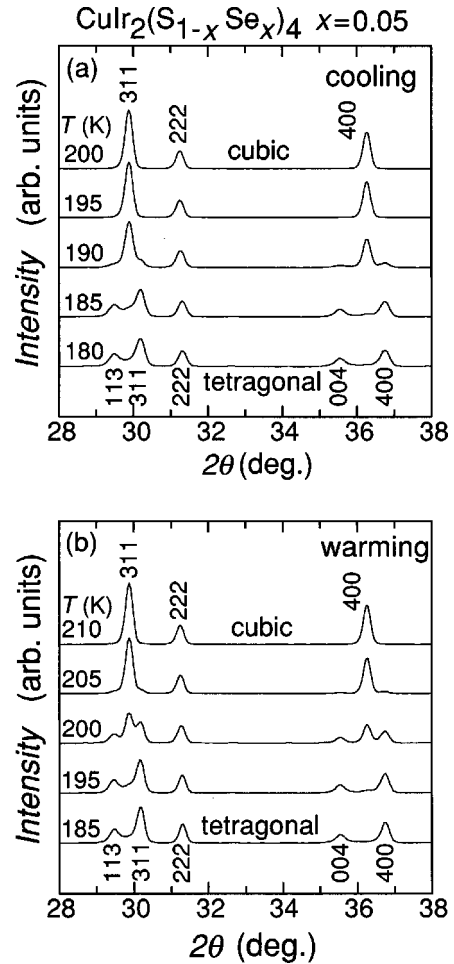

FIG. 6. Temperature dependence of the powder x-ray diffraction pattern for $x = 0.05$: (a) upon cooling and (b) upon warming.

and correspond to the M-I transition in the resistivity data. The magnetic susceptibility of $CuIr_2S_4$ exhibits a sharp jump at 228 K, which is associated with the metal-insulator transition. Measurements were carried out on warming or cooling at a constant applied magnetic field of 10 kOe. Magnetic susceptibilities show the jump at 198, 188, and 175 K for $x = 0.05$, 0.10, and 0.15, respectively. Low-temperature Curie behavior arises from the existence of localized spins of unpaired electrons at lattice imperfections due presumably to sulfur defects or isolated magnetic impurities. It should be noted that the intrinsic localized magnetic moment disappears in the insulating phase except the apparent extrinsic moment mentioned above.

The metallic phase shows Pauli paramagnetism, where the slight increase with increasing temperature is observed in χ for each specimen. The Pauli paramagnetism for the metallic state is evaluated from the difference of the magnitude of the susceptibility due to the opening of the energy gap at the M-I transition. The value of the density of states at the Fermi level, $D(\epsilon_F)$, is extracted from the value of the difference at the transition using the relation $\Delta\chi = \mu_B^2 D(\epsilon_F)$, where μ_B is the Bohr magneton. The values of $D(\epsilon_F)$ are obtained to be 0.67, 0.60, 0.34, and 0.22 states/eV atom for $x = 0.00$, 0.05, 0.10, and 0.15, respectively.

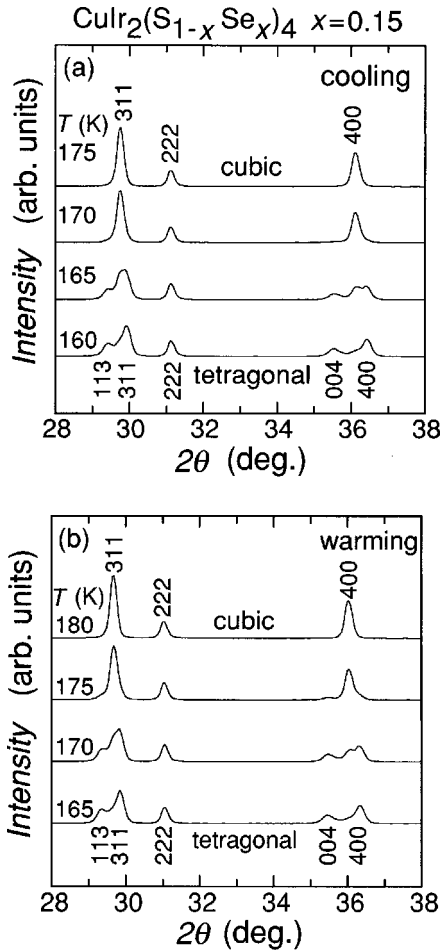FIG. 7. Temperature dependence of the powder x-ray diffraction pattern for $x=0.15$: (a) upon cooling and (b) upon warming.

FIG. 8. Electrical resistivity, ρ, of sintered specimens $CuIr_2(S_{1-x}Se_x)_4$ as a function of temperature.

Below the transition temperature the presence of a temperature-independent diamagnetic term is clear and evaluated to be -6.33×10^{-5} emu mol^{-1} for $CuIr_2S_4$. The susceptibility χ_{core} of the orbital diamagnetism contribution due to ion cores for $Cu^+Ir^{3+}Ir^{4+}S_4{}^{2-}$ is estimated to be -2.26×10^{-4} emu mol^{-1}, and this value is a reasonable one.[34] Figure 14 indicates the susceptibility data for $0.20 \leq x \leq 1.00$. Broad and gradual change in the susceptibility are clearly observed for $x=0.20$ and 0.50, and the inflection points are approximately 180 and 150 K, respectively. The large increase in the susceptibility at low temperatures appears to be caused mainly by extrinsic paramagnetic impurities that arise from the defect with magnetic state. Then, there is no intrinsic localized magnetic moment. For example, the effective magnetic moment per molecule from the value of the Curie constant is about 0.093 μ_B, for $x=0.50$, which is much less than the spin-only moment 1.73 μ_B expected for $S=1/2$.

The disappearance of localized magnetic moment in the insulating phase may be attributed to forming nonmagnetic singlet spin pairs in the dimers, while the small number of reminders of site without pairing might also be paramagnetic. The minority Ir^{4+} sites are magnetically localized in the spin singlet matrix. Doping with Se ions is thought to perturb the lattice and to break up some of the pairs. Nevertheless, a systematic pr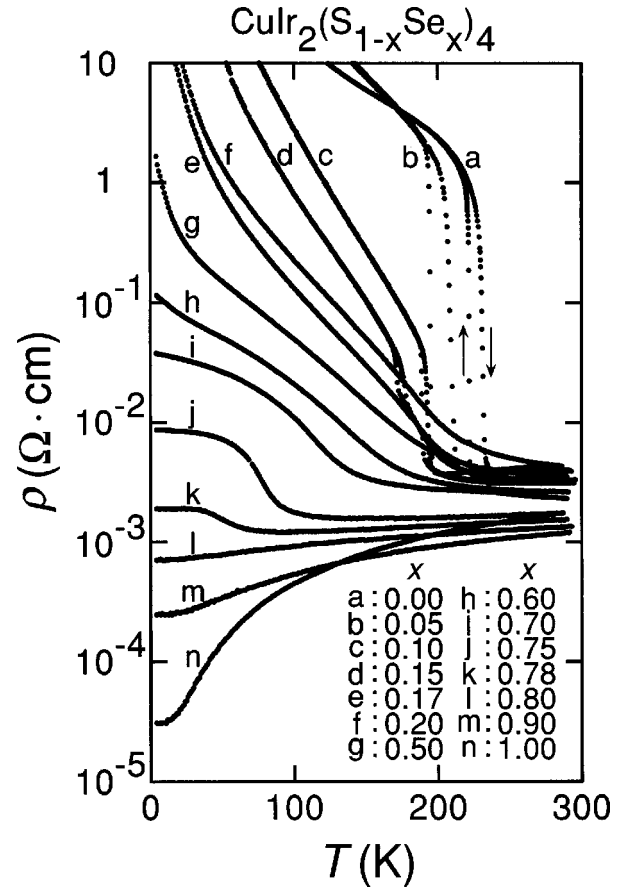oduction of concomitant increase due to the pair breaking in the susceptibility has not been observed at low temperature. Therefore, the pairing seems to be tight and strong.

The temperature-independent magnetic susceptibility χ_0 is very sensitive to Se concentration x in the higher-concentration regime as shown in Fig. 14. In the insulating phase the value of χ_0 may be influenced by the variation of the Van Vleck contribution originated from the Ir ions.

D. Phase diagram

A phase diagram for temperature versus concentration is shown in Fig. 15. Both of the temperature- and concentration-induced M-I transitions have been seen. The structure change from cubic to tetragonal symmetry has occurred in the range of $0.0 \leq x \leq 0.15$. The dashed curve between the semiconductive B and C phases indicates the vague shoulder points in the resistivity, which refer to the inflection points for $x=0.70$, 0.75, and 0.78. Figure 16 shows the temperature derivative $d\rho/dT$ curve as a function of temperature for $0.60 \leq x \leq 0.78$. The transition, if it exists, is likely higher order for $0.17 \leq x \leq 0.78$ without the structural transformation. Here, it is noted that we have not measured the temperature hysteresis effect in the resistivity for this concentration range. Furthermore, according to the recent NMR study by Tsuji *et al.*,[35,36] there exists a clear anomaly in the Knight shift around the dashed curve. They have discussed these anomalies in conjunction with the volume change effect in this system of $CuIr_2(S_{1-x}Se_x)_4$. A
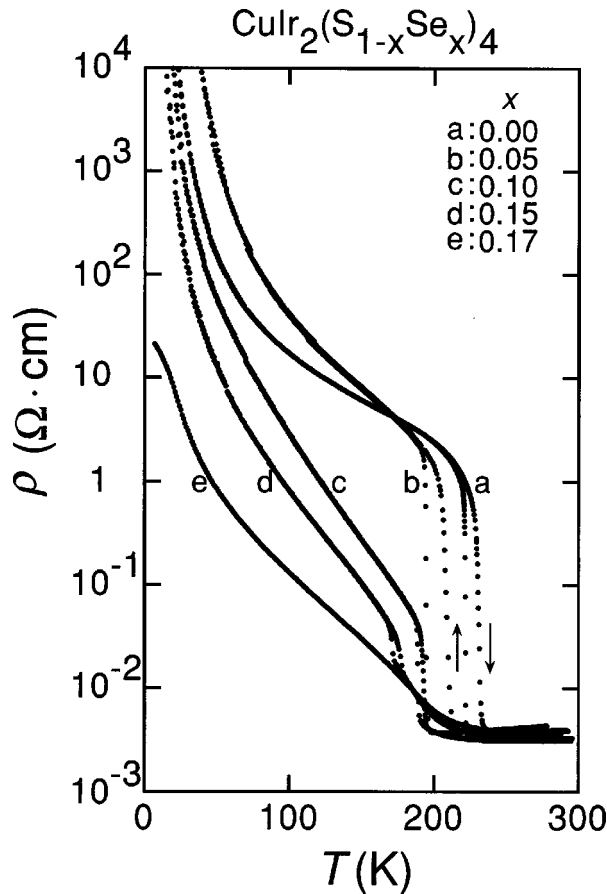
FIG. 9. Expanded plots of the electrical resistivity in the insulator phase of $CuIr_2(S_{1-x}Se_x)_4$ as a function of temperature for the concentration range over $0.0 \leq x \leq 0.17$: in the resistivity range of 10^{-3} to 10^4 Ω cm.

FIG. 10. Expanded plots of the electrical resistivity in the metallic phase of $CuIr_2(S_{1-x}Se_x)_4$ as a function of temperature for the concentration range over $0.0 \leq x \leq 0.17$: in the resistivity range of 10^{-3}–10^{-1} Ω cm.

significant conclusion arising from these results is that the M-I transition is first order in the range $x \leq 0.15$ accompanied by the structural transformation and is second (or higher) order for $0.17 \leq x \leq 0.78$; further, no transition is found for $x \geq 0.80$.

E. ^{193}Ir Mössbauer spectra

The ^{193}Ir Mössbauer spectra of $CuIr_2S_4$ taken at various temperatures in the insulating tetragonal phase are shown in Fig. 17. The high energy of the Mössbauer transition did not allow measurements in the metallic cubic phase ($T_{M-I} = 226$ K) owing to the rapid decrease of the recoilless fraction (the Debye-Waller factor) with increasing temperature. The Mössbauer spectrum of $CuIr_2Se_4$ recorded at 4.2 K is presented in Fig. 18, where it is compared to the spectrum of $CuIr_2S_4$ obtained at the same temperature. Notice that in contrast to the sulfide, the selenide sample remains metallic down to 4.2 K and keeps the cubic symmetry of spinel structure.[16]

The spectra of both $CuIr_2S_4$ and $CuIr_2Se_4$ consist basically of two broad lines of equal intensity. This leads us to consider first a single Ir site model; i.e., all of the Ir ions occur in the same charge state. The Ir ions can experience either a magnetic hyperfine field and/or an electric-field gradient. The occurrence of a magnetic interaction could be expected, e.g., for tetravalent Ir. This possibility was, however,
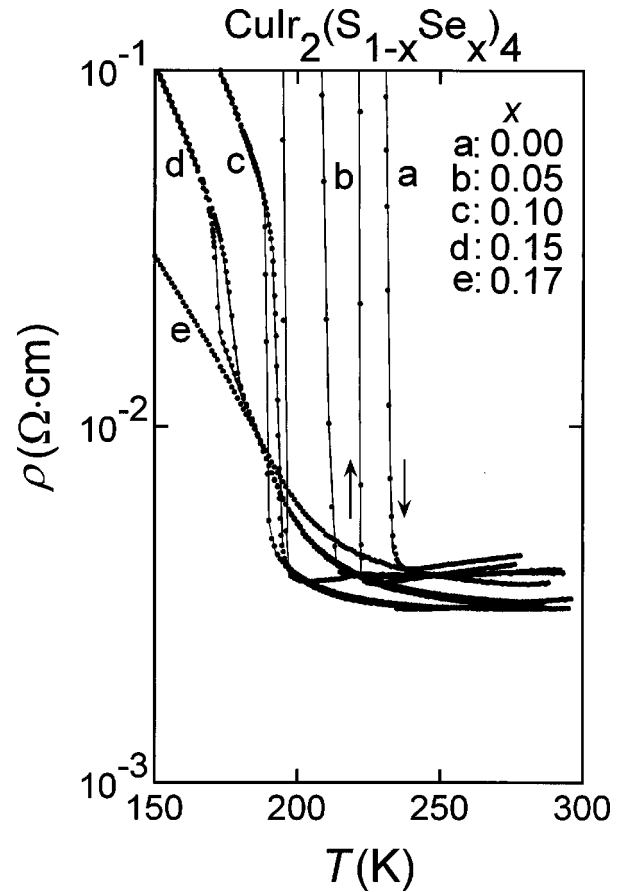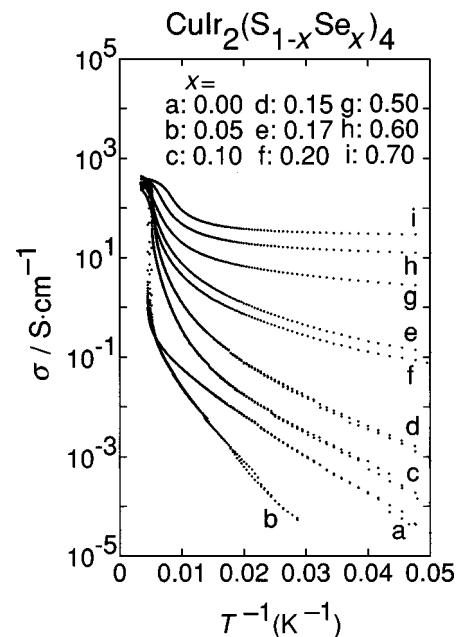

FIG. 11. The conductivity, σ, of $CuIr_2(S_{1-x}Se_x)_4$ plotted against $1/T$ for the concentration range over $0.0 \leq x \leq 0.70$.

TABLE I. Summary of numerical values of the activation energy q and the preexponential factor A in the expression of $\sigma = A \exp(-q/k_B T)$ for the various x in $CuIr_2(S_{1-x}Se_x)_4$. These values, which include considerable experimental errors, are extracted from the data over a temperature range of 200–300 K.

x	q (eV)	A (10^2 S cm^{-1})
0.10	0.009	4.87
0.15	0.025	9.04
0.17	0.024	7.80
0.20	0.045	15.3
0.50	0.023	7.43
0.60	0.010	5.74
0.70	0.011	6.63

ruled out from the analysis of the spectral shape and from the fact that the overall splitting of the doublet is temperature independent, see Fig. 17. This conclusion agrees well with both the diamagnetic behavior observed in $CuIr_2S_4$ below T_{M-I} and the Pauli paramagnetism of $CuIr_2Se_4$.[3,16] The analysis assuming a single quadrupolar interaction is reported in Table II. It is found that the quadrupole coupling constants e^2qQ are rather large even for distorted octahedral environments (e.g., the electric-field gradient eq amounts to 1.7×10^{22} V/m^2 for $CuIr_2S_4$). In addition, the linewidths (W) observed for $CuIr_2S_4$ are broader than generally accepted ($W \approx 0.8$ mm/s).

In a second step, the Mössbauer data were analyzed by assuming that the Ir ions are stabilized in two different charge states (two sites model), i.e., each peak of the doublet is assigned to a different valence state of the Ir ions. The results of the fitting procedure are reported in Table II. This two sites model leads to an important result; that is, the relative population (ratio of the spectral areas) for the two valence states is found to be 1:1, within our experimental error.
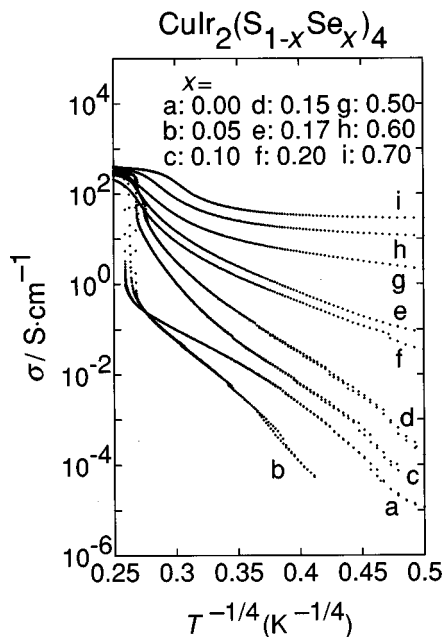

FIG. 12. The conductivity, σ, of $CuIr_2(S_{1-x}Se_x)_4$ plotted against $T^{-1/4}$ for the concentration range over $0.0 \leqslant x \leqslant 0.70$.
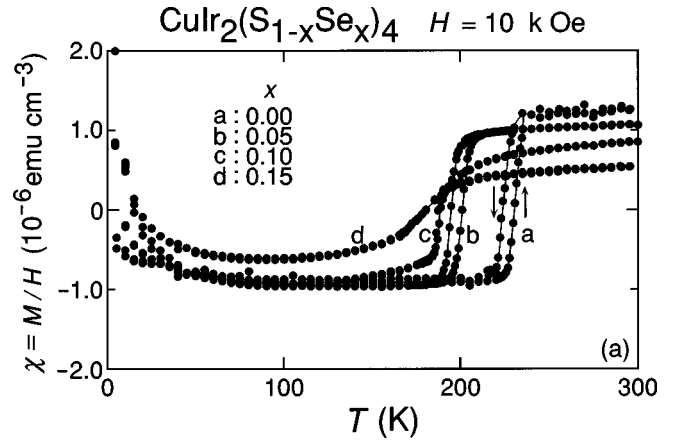

FIG. 13. Magnetic susceptibility vs temperature for powder specimens of $CuIr_2(S_{1-x}Se_x)_4$ as a function of temperature for the concentration range over $0.0 \leqslant x \leqslant 0.15$.

The other important parameter is the isomer shift (δ_{IS}) because it allows us, generally, to assign, at least in insulating compounds, a charge state to the Ir ions.[30] Figure 19 taken from reference by Demazeau *et al.*,[29] indicates that the isomer shifts of oxides and halides vary gradually with the Ir valence state and that different Ir compounds with the same valence state cluster in rather well-defined regions; This is because the shielding of s electrons, which contributes directly to the electron density, $\rho(0)$, at the Ir nuclei, is reduced when d electrons are removed, i.e., when the Ir valence state increases. The increase of δ_{IS} or of $\rho(0)$ for a given charge state from halides to oxides is related to covalence effects. For $CuIr_2S_4$, the assignment of the valence state $Ir^{5+}(5d^4)$, $\delta_{IS} = +0.82$ mm/s versus Ir metal, and $Ir^{3+}(5d^6)$, $\delta_{IS} = -1.90$ mm/s versus Ir metal, is concluded from the isomer shift systematics established for Ir compounds as shown in Fig. 19. It is worth mentioning that neither $Ir^{5+}(t_{2g}^4 e_g^0)$ nor $Ir^{3+}(t_{2g}^6 e_g^0)$ in their low spin states possess a magnetic ground state in the low-temperature tetragonal phase. The occurrence of Ir^{5+} and Ir^{3+} ions in the insulating phase of $CuIr_2S_4$ is at first sight surprising because it implies that the Cu charge state should be zero. One should, however, consider that covalency plays an important
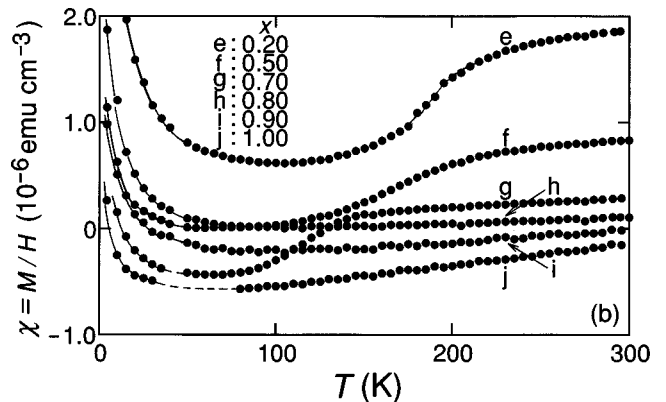

FIG. 14. Magnetic susceptibility vs temperature for powder specimens of $CuIr_2(S_{1-x}Se_x)_4$ as a function of temperature for the concentration range over $0.20 \leqslant x \leqslant 1.0$.
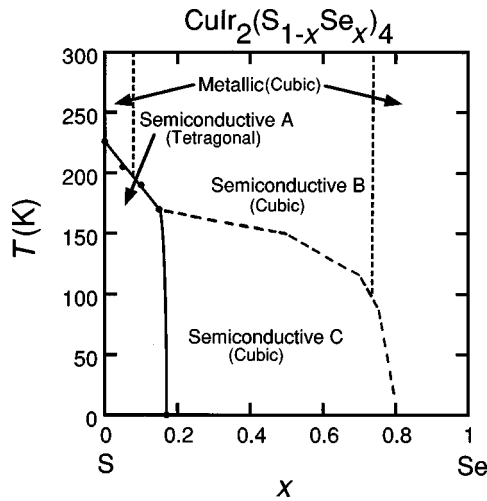
FIG. 15. A phase diagram for temperature vs concentration x. The dashed curve indicates the vague boundary in the semiconductive region, see text.

role in the bonding with the sulfur ligand. The significance of the formal valence state in such compounds should be examined in more detail.

As shown in Table II, the Mössbauer data of $CuIr_2Se_4$ can be analyzed straightforwardly by assuming either a single-Ir-site or a two-Ir-site model. However, the expected increase of δ_{IS} is not observed in the latter model when one moves from the sulfides to the selenides (actually δ_{IS} increases only for one charge state). In contrast, the single-site model points to the occurrence of tetravalent Ir. The isomer shift of -0.67 mm/s follows the expected trends, but remember that $CuIr_2Se_4$ is metallic. The assignment of an Ir^{4+} charge state can thus be questionable.

In conclusion, with regard to the ^{193}Ir Mössbauer spectra, it is conjectured that the Ir ions are in a mixed valence state (formal Ir^{3+} and Ir^{5+} charge states) in the insulating phase of $CuIr_2S_4$. In contrast to $CuIr_2S_4$, a single charge state (possibly Ir^{4+}) is anticipated in metallic $CuIr_2Se_4$.
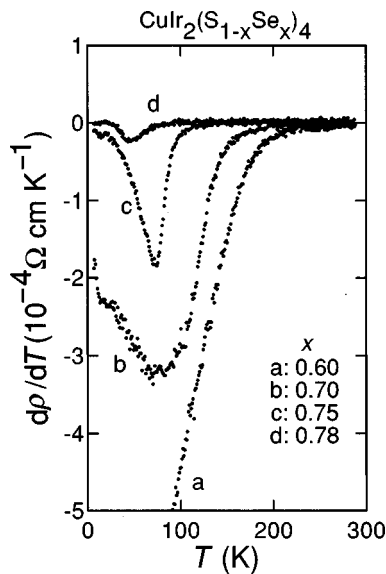

FIG. 16. Temperature derivative $d\rho/dT$ curve as a function of temperature for $0.60 \leqslant x \leqslant 0.78$.
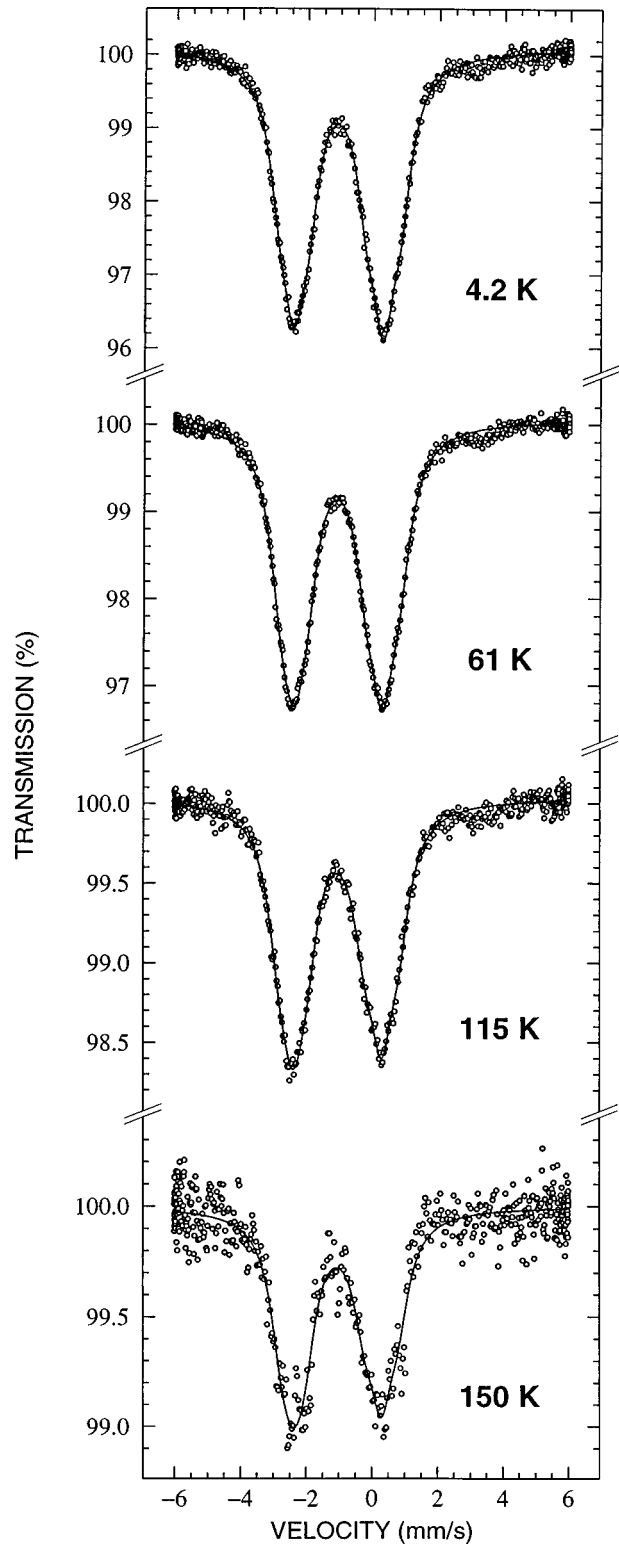

FIG. 17. ^{193}Ir Mössbauer spectra of $CuIr_2S_4$ as a function of relative velocity between source and absorber taken at different temperatures in the insulating tetragonal phase.

F. Change of the M-I transition from first order to higher order

In common with mixed valence compounds, most physical properties are profoundly influenced by changes of concentration in cation oxidation states, associated with departures from ideal metal-oxygen stoichiometry, in the
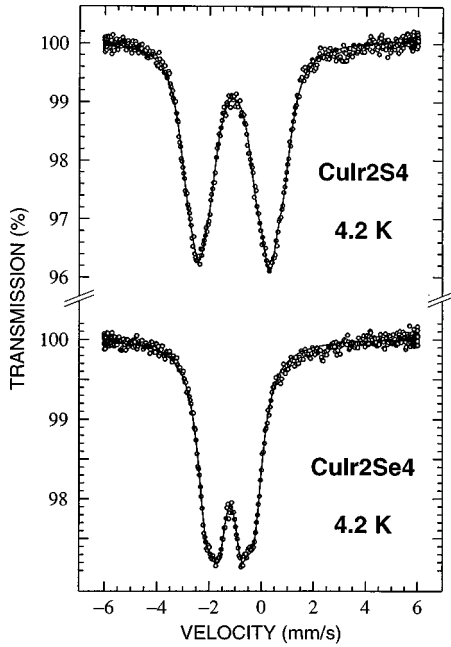
FIG. 18. ^{193}Ir Mössbauer spectra of $CuIr_2S_4$ and $CuIr_2Se_4$ as a function of relative velocity between source and absorber taken at 4.2 K. The latter compound is metallic and has a cubic normal spinel structure.

transition-metal oxides. The Verwey transition in the magnetite $Fe_{3(1-\delta)}O_4$, where δ indicates the deviation of the oxygen-to-metal ratio, has been the subject of a large number of studies. The transition from first order to higher order with increasing δ has been extensively analyzed by Honig and co-workers[37–41] and developed by Koga,[42–44] based on the two-state approximation formulated by original Strässler and Kittel theory.[45,46] This simple mean-field model describes the gross aspects of the observed anomalous behavior in $Fe_{3(1-\delta)}O_4$. The discontinuous Verwey transition is driven by a change in a highly correlated electron system with tem-

TABLE II. Hyperfine interaction parameters for ^{193}Ir in $CuIr_2S_4$ and $CuIr_2Se_4$ at 4.2 K. e^2qQ is the quadrupole coupling constant, δ_{IS} is the isomer shift with respect to Ir metal, and W is the linewidth of the Lorentzian lines. Summary of the results obtained from the single-site model and from the two-site model. It should be noted that $CuIr_2S_4$ is insulating at 4.2 K and has a tetragonal structure induced by the metal-insulator transition at 226 K. $CuIr_2Se_4$ is metallic with a normal cubic spinel structure.

$CuIr_2S_4$	Single-site model	Two-site model	
δ_{IS} (mm/s)	$-0.53(1)$	$+0.82(2)$	$-1.90(3)$
e^2qQ (mm/s)^{a,b}	$5.46(3)$	$1.05(3)$	$0.78(3)$
W (mm/s)	$1.17(3)$	$0.82(4)$	

$CuIr_2Se_4$	Single-site model	Two-site model	
δ_{IS} (mm/s)	$-0.67(1)$	$+0.00(2)$	$-1.35(2)$
e^2qQ (mm/s)^{a,b}	$2.70(2)$	~ 0	~ 0
W (mm/s)	$0.80(2)$	$0.80(2)$	

^{a}1 mm/s = 58.91 MHz.
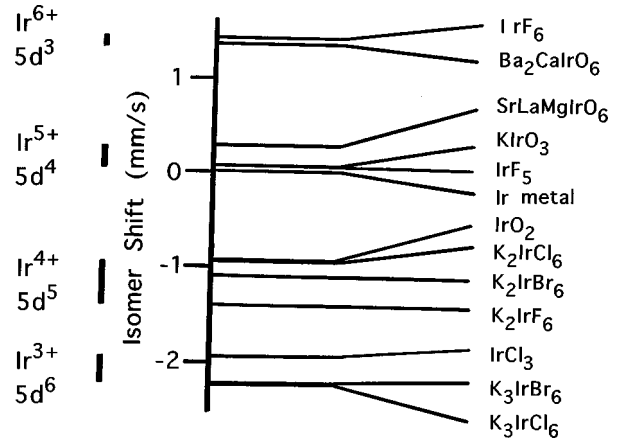$^b eq$ (V/m^2) = $3.12 \times 10^{21} e^2qQ$ (mm/s).

FIG. 19. ^{193}Ir isomer shifts for various iridium oxide and halide compounds. The shifts are given with respect to Ir metal (adapted from Ref. 29).

perature from a charge-ordered small-polaron state associated with local lattice deformations to a disordered state in which electrons resonate between Fe^{2+} and Fe^{3+} ions located on the B sites.

The ionic state is $Cu^+ Ir^{3+} Ir^{4+} S_4^{2-}$ in the insulating phase of $CuIr_2S_4$. The magnetic state of Ir^{3+} is nonmagnetic with $S=0$ while Ir^{4+} has $S=1/2$ in the low-spin state for the $d\epsilon$ level with a small tetragonal distortion.

In the system of $CuIr_2(S_{1-x}Se_x)_4$, the Se substitution for S sites suppresses the M-I transition and changes transition from the first-order to the higher-order one. The gross aspect of the observed results in $CuIr_2(S_{1-x}Se_x)_4$ could be interpreted in the same framework of the Strässler and Kittel theory.[45] In the framework of this theory, the first-, second-, and higher-order transitions are treated in an unified scheme, in which free energy is written in terms of the order parameter for the two-level scheme. However, we do not describe the detailed and sophisticated model calculations because the charge ordering state is not verified yet experimentally for this system of $CuIr_2(S_{1-x}Se_x)_4$. It is planned to present a paper in more detail elsewhere in the future.

It should be pointed out that the M-I transition temperature increases rather rapidly by the application of pressure.[3,9] This is unlikely and inconsistent with the possibility of Wigner crystallization, in which the transition temperature is expected to decrease with an increase of the carrier density due to the shielding effect of Coulomb interaction by the conduction electron.

IV. SUMMARY

The following facts have been clarified. (1) $CuIr_2S_4$ has a normal spinel structure. The metal-insulator transition temperature T_{M-I} of $CuIr_2S_4$ is 226 K at the midpoint in the temperature interval of the hysteresis spread about 10 K. (2) With decreasing temperature through T_{M-I}, the structure transforms from cubic to tetragonal with a volume contraction of 0.7%. The tetragonal phase has an axial ratio $c/a = 1.03$. It is stressed that the volume of low-temperature insulating phase is smaller than that of high-temperature metallic phase. (3) The enthalpy and entropy of the M-I transition of $CuIr_2S_4$ are 3.50 kJ mol^{-1} and 15.6 JK^{-1} mol^{-1}, respectively. (4) The insulating phase in $CuIr_2S_4$ shows ac-

tivated conduction with an activation energy of 47 meV between 140 and 200 K. On the other hand, photoemission spectra near the Fermi level show a gap of ~ 20 meV opening. (5) The metallic phase of $CuIr_2S_4$ indicates Pauli paramagnetism and the density of states at the Fermi level is estimated to be 0.67 states/eV atom. (6) The localized magnetic moment seems not to exist in the insulating phase of $CuIr_2S_4$. Low-temperature Curie-like behavior arises from magnetic impurities. (7) Cu-NMR measurements and photoemission spectra confirm that the Cu ion is in the monovalent state in the insulating phase of $CuIr_2S_4$, which is supported by energy band calculation. Then, Ir has a mixed-valence state formally. (8) The explanation of the Jahn-Teller distortion originated from the Cu^{2+} ion at the tetrahedral A site is not correct because the ionic state is Cu^+.[47–50] (9) The ^{193}Ir Mössbauer spectra in $CuIr_2S_4$ and $CuIr_2Se_4$ show two clear absorption lines. Unfortunately no conclusion is reached as to whether the one-site or two-site model is relevant. It is hoped that the value of e^2qQ is determined with NQR or NMR measurements. (10) The ionic state is $Cu^+Ir^{3+}Ir^{4+}S_4^{2-}$ in the insulating phase of $CuIr_2S_4$. The magnetic state of Ir^{3+} is nonmagnetic with $S=0$ while Ir^{4+} has $S=1/2$ in the low-spin state for the $d\epsilon$ level with a small tetragonal distortion. (11) A possibility of formation of spin singlet Ir^{4+}-Ir^{4+} pairs in the insulating phase has been pointed out. The substitution of Se ions for S ions may not break up Ir^{4+}-Ir^{4+} pairs, neither does this substitution perturb the neighboring Ir^{4+}-Ir^{4+} units. However, no experimental verification for the dimerization with the spin singlet has yet, to our knowledge, been presented. (12) On the other hand, $CuIr_2Se_4$ remains metallic down to 0.5 K without the transition. (13) A phase diagram of between temperature and Se concentration x has been determined experimentally for a system of $CuIr_2(S_{1-x}Se_x)_4$. The transport and magnetic inherent prop-

erties seem to change gradually with x. (14) The M-I transition of $CuIr_2(S_{1-x}Se_x)_4$ for $x \leq 0.15$ is accompanied by a structural transformation from tetragonal (low-temperature insulating phase) to cubic (high-temperature metallic phase) symmetry. (15) The Arrhenius regime is observed for the conductivity with a thermally activated process for $0 \leq x \leq 0.70$. The metallic conductivity recovers for $x \geq 0.80$. (16) Magnetic susceptibility shows the jump at $T_{M\text{-}I}$. From the height in this jump, density of states at the Fermi level, $D(\epsilon_F)$, is estimated, in which the value decreases with x. (17) The large increase in the susceptibility at low temperature appears to be caused by paramagnetic impurities. There is no intrinsic localized magnetic moment.

In summary, the mechanism of the M-I transition in $CuIr_2(S_{1-x}Se_x)_4$ remains enigmatic. We hope to investigate this question to obtain the complete picture. In particular, the detailed structure analysis such as the superstructure in the insulating phase of $CuIr_2S_4$ is important to clarify the charge ordering. An extensive study of the detailed structure analysis can be found elsewhere.[51]

*Author to whom correspondence should be addressed. Electronic address: naga-sho@oyna.cc.muroran-it.ac.jp

[1] *Ferro-Magnetic Materials,* edited by E. P. Wohlfarth, A Handbook on the Properties of Magnetically Ordered Substances Vol. 3 (North-Holland, Amsterdam, 1982), p. 603.

[2] S. Nagata, T. Hagino, Y. Seki, and T. Bitoh, Physica B **194-196**, 1077 (1994).

[3] T. Furubayashi, T. Matsumoto, T. Hagino, and S. Nagata, J. Phys. Soc. Jpn. **63**, 3333 (1994).

[4] J. Matsuno, T. Mizokawa, A. Fujimori, D. A. Zatsepin, V. R. Galakhov, E. Z. Kurmaev, Y. Kato, and S. Nagata, Phys. Rev. B **55**, R15 979 (1997).

[5] K. Kumagai, S. Tsuji, T. Hagino, and S. Nagata, in *Spectroscopy of Mott Insulators and Correlated Metals*, Springer Series in Solid-State Sciences, Vol. 119, edited by A. Fujimori and Y. Tokura (Springer-Verlag, Berlin, 1995), p. 255.

[6] T. Oda, M. Shirai, N. Suzuki, and K. Motizuki, J. Phys.: Condens. Matter **7**, 4433 (1995).

[7] T. Oda, M. Shirai, N. Suzuki, and K. Motizuki, Cryst. Res. Technol. **31**, 877 (1996).

[8] T. Hagino, T. Tojo, T. Atake, and S. Nagata, Philos. Mag. B **71**, 881 (1995).

[9] G. Oomi, T. Kagayama, I. Yoshida, T. Hagino, and S. Nagata, J. Magn. Magn. Mater. **140-144**, 157 (1995).

[10] E. J. W. Verwey and P. W. Haayman, Physica (Amsterdam) **8**, 979 (1941).

[11] E. J. W. Verwey and E. L. Heilmann, J. Chem. Phys. **15**, 174 (1947).

[12] E. J. W. Verwey, P. W. Haayman, and F. C. Romeijn, J. Chem. Phys. **15**, 181 (1947).

[13] L. R. Bickford, Jr., Rev. Mod. Phys. **25**, 75 (1953).

[14] P. A. Miles, W. B. Westphal, and A. von Hippel, Rev. Mod. Phys. **29**, 279 (1957).

[15] S. Chikazumi, in *Magnetism and Magnetic Materials*, edited by J. J. Becker, G. H. Lander, and J. J. Rhyne, AIP Conf. Proc. No. 29 (AIP, New York, 1976), p. 382.

[16] T. Hagino, Y. Seki, and S. Nagata, Physica C **235-240**, 1303 (1994).

[17] T. Furubayashi, T. Kosaka, J. Tang, T. Matsumoto, Y. Kato, and S. Nagata, J. Phys. Soc. Jpn. **66**, 1563 (1997).

[18] N. H. Van Maaren, G. M. Schaeffer, and F. K. Lotgering, Phys. Lett. **25A**, 238 (1967).

[19] M. Robbins, R. H. Willens, and R. C. Miller, Solid State Commun. **5**, 933 (1967).

[20] R. N. Shelton, D. C. Johnston, and H. Adrian, Solid State Commun. **20**, 1077 (1976).

[21] T. Hagino, Y. Seki, N. Wada, S. Tsuji, T. Shirane, K. I. Kumagai, and S. Nagata, Phys. Rev. B **51**, 12 673 (1995).

[22] T. Bitoh, T. Hagino, Y. Seki, S. Chikazawa, and S. Nagata, J. Phys. Soc. Jpn. **61**, 3011 (1992).

[23] T. Shirane, T. Hagino, Y. Seki, T. Bitoh, S. Chikazawa, and S. Nagata, J. Phys. Soc. Jpn. **62**, 374 (1993).

[24] S. Nagata, S. Yasuzuka, Y. Kato, T. Hagino, N. Matsumoto, N. Kijima, and S. Ebisu, in *Proceedings of the International Conference on Low Temperature Physics, LT21, Prague, August 1996,* edited by S. Danis, V. Gregor, and K. Zaveta [Czech. J. Phys. 46 (Suppl), 2425 (1996)].

[25] N. Matsumoto, H. Honma, Y. Kato, S. Yasuzuka, K. Morie, N. Kijima, S. Ebisu, and S. Nagata, in *Proceedings of the 9th International Symposium on Superconductivity, Sapporo, Japan, Oct. 1996,* edited by S. Nakajima and M. Murakami [Adv. Supercond. **9**, 175 (1997)].

[26] N. Kijima, H. Yashiro, and S. Nagata, J. Phys. Chem. Solids **57**, 1635 (1996).

[27] P. Kichambare, N. Kijima, H. Honma, S. Ebisu, and S. Nagata, J. Phys. Chem. Solids **57**, 1615 (1996).

[28] N. Kijima, P. D. Kichambare, H. Honma, S. Ebisu, and S. Nagata, Physica C **263**, 523 (1996).

[29] G. Demazeau, D. Y. Jung, J. P. Sanchez, E. Colineau, A. Blaise, and L. Fournes, Solid State Commun. **85**, 479 (1993).

[30] F. E. Wagner, Hyperfine Interact. **13**, 149 (1983).

[31] N. F. Mott, Philos. Mag. **19**, 835 (1969).

[32] J. R. Drabble, T. D. Whyte, and R. M. Hopper, Solid State Commun. **9**, 275 (1971).

[33] *Hopping Transport in Solids,* edited by M. Pollak and B. I. Shklovskii, Modern Problems in Condensed Matter Science Vol. 28 (North-Holland, Amsterdam, 1991), p. 18.

[34] *Magnetic Properties of Coordination and Organometallic Transition Metal Compounds,* edited by K.-H. Hellwege and A. M. Hellwege, Landolt-Börnstein, New Series, Group II, Vol. 8 (Springer-Verlag, Berlin, 1976), p. 27.

[35] S. Tsuji, K. Kumagai, N. Matsumoto, Y. Kato, and S. Nagata, Physica B **237-238**, 156 (1997).

[36] S. Tsuji, K. Kumagai, N. Matsumoto, and S. Nagata, Physica C **282-287**, 1107 (1997).

[37] J. M. Honig, Phys. Chem. Miner. **15**, 476 (1988).

[38] R. Aragón and J. M. Honig, Phys. Rev. B **37**, 209 (1988).

[39] J. M. Honig and J. Spalek, J. Less-Common Met. **156**, 423 (1989).

[40] J. M. Honig, J. Spalek, and P. Gopalan, J. Am. Ceram. Soc. **73**, 3225 (1990).

[41] J. M. Honig and J. Spalek, J. Solid State Chem. **96**, 115 (1992).

[42] S. Takai, T. Atake, and Y. Koga, Thermochim. Acta **246**, 1 (1994).

[43] Y. Koga, Chem. Phys. Lett. **31**, 571 (1975).

[44] Y. Koga, Collect. Phenom. **3**, 1 (1978).

[45] S. Strässler and C. Kittel, Phys. Rev. **139**, A758 (1965).

[46] D. B. Chesnut, J. Chem. Phys. **40**, 405 (1964).

[47] H. A. Jahn and E. Teller, Proc. R. Soc. London, Ser. A **161**, 220 (1937).

[48] J. H. Van Vleck, J. Chem. Phys. **7**, 72 (1939).

[49] J. D. Dunitz and L. E. Orgel, J. Phys. Chem. Solids **3**, 20 (1957).

[50] U. Öpik and M. H. L. Pryce, Proc. R. Soc. London, Ser. A **238**, 425 (1957).

[51] T. Kimoto *et al.* (unpublished).